# 3D-Hepatocellular Carcinoma (3D-HCC) Models of Diffused and Aggregated Spheroids using a 96-Pillar/Well Plate

**Sangyun Lee**
Department of Health Science and Technology, Samsung Advanced Institute for Health Sciences and Technology (SAIHST), Sungkyunkwan University

**Yvonne Teng**
AVATAMED Pte. Ltd.,

**Miseol Son**
AVATAMED Pte. Ltd.

**Bosung Ku**
Medical & Bio Device (MBD) Co., Ltd.

**Hyun Ju Whang**
MBDA UK Ltd: MBDA Holding SAS

**Vinay Tergaonkar**
IMCB: Institute of Molecular and Cell Biology

**Pierce Kah-Hoe Chow**
NCCS: National Cancer Centre Singapore

**Dong Woo Lee** ( dw2010.lee@gmail.com )
Konyang University

**Do-Hyun Nam**
Sungkyunkwan University School of Medicine

**Research**

**Keywords:** 3D cell culture, Hepatocellular carcinoma (HCC) cell line, in vitro extra cellular matrix (ECM) remodeling, Cancer spheroids in Matrigel, High-Throughput Screening (HTS), 96Pillar/Well Plate

**Posted Date:** February 19th, 2021

**DOI:** https://doi.org/10.21203/rs.3.rs-218522/v1

# Abstract

**Background:** Hepatocellular carcinoma (HCC) is the sixth most common cancer and the third most frequent cause of cancer-related mortality worldwide. The genetic and physiological complexity of HCC is a major barrier to the study of tumorigenesis and identification of therapeutic targets. The three-dimensional (3D) culture of cancer cells within an extracellular matrix (ECM) provides an in vitro tumor model that best recapitulates in vivo tumor pathophysiology.

**Methods:** In the current study, we cultured cells and made spheroids by aggregating cells or diffusing cells in Matrigel attached on the tip of the 96-pillar plate. According to the initial cell position in Matrigel, two 3D-HCC cancer in-vitro models (diffused spheroid model and aggregated spheroid model) were established. These two models were applied to drug sensitivity assays to identify drug sensitivity changes. The protein expression and cytokine activation related to the drug resistance and maintenance of the physiological properties of HCC cells were analyzed in both models. This 3D culture method not only maintained the phenotype of the tumor but allowed easy high-throughput screening (HTS) due to its 96-array plate configuration.

**Results:** The Aggregated Spheroid Model (ASM) showed higher expression of cancer markers associated with proliferation, tight junctions formation and epithelial cell identity in HCC cells, as well as cytokine factors associated with immune cell recruitment/activation, ECM regulation, cancer interaction, and angiogenesis regulation.

**Conclusions:** Overall, the proposed ASM better recapitulates the tumor microenvironment, demonstrating the involvement of the ECM/tight junctions in the cell-to-cell signaling processes. This provides more instructive data for in vitro screening of tumor cells.


# Background

Hepatocellular carcinoma (HCC) is the sixth most common cancer and the third most frequent cause of cancer-related mortality worldwide [1–3]. The genetic and physiological complexity of HCC is a major barrier to the study of tumorigenesis and identification of therapeutic targets. Sorafenib is a drug that is the standard of care for patients in advanced stage HCC, and Regorafenib is recommended as a second-line therapy in patients who are nonresponsive but tolerant to Sorafenib [4–6]. Sorafenib [7–8] and Regorafenib [9–11] are small, novel oral multikinase inhibitors that were developed to target different tyrosine kinases involved in the angiogenic, tumor growth-promoting, and tumor microenvironment signaling pathways, including the Ras/Raf/MEK/ERK pathway, vascular endothelial growth factor receptors (VEGFR1, 2, and 3), platelet-derived growth factor receptor beta (PDGFR-β), and fibroblast growth factor receptor 1 (FGFR1).

However, HCC patients typically have poor tolerance of systemic chemotherapy due to underlying chronically damaged tissue and liver dysfunction that contains considerable inflammation, fibrosis, and cirrhosis. Therefore, to find the most responsive and effective drug for HCC patients, many preclinical

studies and *in vitro* drug assays are conducted using patient derived tumor cells grown under two-dimensional (2D) monolayer cell culture conditions. The conventional 2D cell culture system is well established and generates highly reproducible data. Due to these opportunities, high-throughput screening (HTS) methods have been widely used for scientific experimentation. However, particularly in the field of drug discovery, its limitations have been increasingly recognized. The conventional 2D cell culture-based HTS platform does not reflect the actual patient's tumor microenvironment such as physiological cell-to-cell and cell-to-extracellular matrix (ECM) interactions [12]. Also, many cells lose some of their actual phenotypic and genomic properties when grown using *in vitro* methods with 2D cell culture. As a result of these limitations, experimental results using 2D cell culture may provide ambiguous and nonpredictive data for *in vivo* and clinical responses [13–15].

There is a need for suitable experimental models to address these limitations. One model that may overcome these issues is the 3D culture model which was devised to better mimic the *in vivo* behavior of tumor cells under more adaptable conditions. In contrast to the 2D culture system, a recent study reported that 3D cultured spheroids composed of patient-derived tumor cells could maintain tumor characteristics *in vitro* for an extended period [16]. Because of the structural and physical differences in dimensionality, 3D cell culture methods have an advantage that leads to differences in the physiological activity of cells. These biological and physical aspects of 3D cell cultures affect not only the expression of the cell surface receptors but also induce the activation of signal transduction from the outside to the inside of cells. Finally, the characteristics of 3D cell culture influence gene expression and cellular responses. It has been reported that 3D cultured cell responses are more similar to *in vivo* testing results compared to those from 2D cell culture [17–18].

To address these issues our research group has developed Pillar/well plates for the 3D cell culture on the surface of the pillar as previously reported [19–24]. Since alginate is easier to handle, our previous 3D cell culture studies were conducted by adopting alginate as an extracellular matrix. Commercially available alginates are extracted from harvested brown seaweeds. Although alginates have been used as biomaterials in biological and pharmaceutical fields, its use in biological experiments is controversial as alginate is not an animal-derived material [25–26].

In this regard, Matrigel is widely used and adapted for the 3D cell culture ECM. Matrigel is a soluble extract of basement membrane proteins derived from the Engelbreth-Holm-Swarm (EHS) tumor that forms a 3D gel at 37 ℃. It is known to enhance biological features reflecting their actual cancer cells malignancy and is related to cell proliferation, differentiation, morphology, gene and protein expression, and cellular responses to external stimuli. Matrigel is typically used in monolayer or thin gel conformations, mainly for short-term analysis such as invasion assays, ranging from few hours to 4 days [27–30]. However, spheroid formation in Matrigel differs depending on the initial cell position. Generally, cells are diffused in Matrigel and form multi-spheroids that are connected. This is the diffused spheroid model (DSM). On other hand, when cells were aggregated in Matrigel, big spheroids are formed. Cells are aggregated on the curvature of the Matrigel spot before gelling with Matrigel, which leads to formation of large spheroids. This is the Aggregated Spheroid Model (ASM).

In this study, our research group adapted Matrigel as the 3D cell culture ECM and optimized gelation methods of the cell-Matrigel mixtures to implement two types of 3D cell culture models. (Diffused Spheroid Model “DSM”, Aggregated Spheroid Model “ASM”). Based on two 3D cell culture models, we conducted drug sensitivity assays in order to select efficacious anti-cancer drugs. We analyzed the proteins and cytokine activations related to drug resistance and maintenance of the physiological properties of HCC cells. Through these experiments, we found that the ASM could provide better *in vivo*-like data.

## Methods

# Preparation of the 96 pillar/well plates

The 96-pillar/well plate was manufactured by plastic injection molding and is a robust and flexible platform for mammalian cell cultures, enzymatic reactions, viral infections, and compound screenings (Fig. 1). The 96-pillar plate is made of polystyrene (PS) and contains 96-pillars (with a 2 mm pillar diameter and 9 mm pillar-to-pillar distance). The 96-pillar plate was coated with poly-L-lysine (PLL) solution to support Matrigel attachment on the hydrophilic pillar surface. The 96-well plate has 96 complementary wells (with a 7 mm well diameter and 9 mm well-to-well distance) and it can be combined (or “stamped”) with a 96-pillar plate to conduct the 3D cell culture and the drug efficacy test. Plastic molding was performed with an injection molder (Sodic Plustech Inc., IL).

# Experimental Procedure of High-Throughput Drug Screening

For high-throughput screening and implementation of 3D cell culture models, 1.5 μL volume of mixtures containing approximately 4000 cells and 50% Matrigel were automatically dispensed onto a 96-pillar plate surface using an ASFA™ Spotter ST (Medical & Bio Device, South Korea). The ASFA™ Spotter ST uses a solenoid valve (The Lee Company, USA) to dispense 1.5 μL droplets of the cell–Matrigel mixture on the 96-pillar plate surface.

After dispensing the cells, two types of 3D cell culture models were implemented (DSM and ASM), as shown in (Fig. 2-a). To implement a DSM model, the icing and gelation steps continued with the pillar surface facing upward (Figs. 2-b and -c). To implement the ASM model, the icing and gelation steps continued with the pillar surface facing down (Figs. 2-d and -e). The 96-pillar plate was combined with the pre-warming culture medium and subjected to an additional stabilization for 10 minutes (Fig. 2-f). The 96-pillar plate containing HCC cells in Matrigel was sandwiched (or “stamped”) with the 96-well plate for 3D cell culture (Fig. 2-g). Each 96 well plate was comprised of 96 wells, each 7 mm in diameter, which contained 200uL of cell culture medium. After the cell-Matrigel mixture was stabilized using each gelation method, 3D cells were observed with an optical microscope and appeared to be evenly spread over the pillar surface in the DSM model. In the ASM model, it was confirmed that cells were aggregated in the center of the pillar surface, as shown in (Fig. 2-k).

The cells needed to be stabilized in the Matrigel spots before being treated with drugs. After stabilizing cells, cell viability was checked by 3d live cell staining using Calcein AM dye (Invitrogen, Carlsbad, CA). Majority of cells were alive based on the level of green fluorescence as shown in (Fig. 2-j). To analyze the efficacy of all six drugs, we designed a dose-response curve (DRC). The 96-well plate was divided into 7 regions. Each region was composed of a 3 × 7 well array corresponding to six different drug doses (including one control) and their triplicates. After treatment with the six different drugs for a period of six days, drug response was analyzed through viability quantification of 3d live cell staining images. As shown in (Fig. 2-j), the area value of 3D live cells differed depending on the drug response.

# Experimental Procedure for Image Scanning and Data analysis

An automatic optical fluorescence scanner (ASFA™ Scanner HE, Medical & Bio Device, South Korea) was used to measure green fluorescence intensities (excitation/emission, 494/517 nm to lasers) on the 96-pillar surface using an 8-bit code among the RGB codes (0–255), as shown in (Fig. 2-j). The ASFA Ez SW (Medical & Bio Device) was used to calculate the total and average green areas of the scanned images of the 3D cultured cells from each 3D cell culture model. To determine drug efficacy, the dose-response curves were plotted using the normalized 3D cell viability values according to the dose of the drugs (GraphPad Prism 8). The half-maximal inhibitory concentration ($IC_{50}$) values were calculated automatically in the XY analysis completed with the GraphPad Prism 8 software. (GraphPad Software, CA)

# Cell culture

Human hepatocellular carcinoma cell lines Hep3B and HepG2 were purchased from the Korean Cell Line Bank (Seoul, South Korea). Both Hep3B and HepG2 were cultured in DMEM medium (Gibco, Grand Island, NY) with 1 μg/mL of puromycin; both media were supplemented with 100 μg/mL of streptomycin, 100 units/mL of penicillin, 250 ng/mL of amphotericin B, and 10% fetal bovine serum. Cell lines were maintained at 37°C in a 5% CO2-humidified atmosphere and passaged every four days. Typically, we use the Hep3B and HepG2 cell lines under 20 passages after thawing the frozen cell stock. Under 20 passages, we observed that the Hep3B and HepG2 cell lines easily formed 3D cells in 50% Matrigel on the chip platform.

# Drugs

Two 3D-HCC cancer in-vitro models (DSM and ASM) were used in drug sensitivity assays to identify drug sensitivity change according to each model. The drugs most commonly used for HCC were selected. Sorafenib (S7397), Cabozantinib (S1119), Lenvatinib (S1164), Regorafenib (S1178), 5-Fluorouracil (5-FU) (S1209), and Doxorubicin (DOX) (S1208) were purchased from Selleckchem (Houston, TX). Drugs were solved in a stock solution of dimethyl sulfoxide (DMSO, 100 mM).

# 3D-Cell Viability Assay

Hep3B and HepG2 cells were seeded in a 96-pillar tray at a density of 4000 cells per pillar in triplicate for each treatment. One day after seeding, cells were treated with drugs in a two-fold and seven-dose point serial dilution from 100 µM to 3.12 µM. After 6 days of incubation at 37°C in a 5%-CO2 humidified incubator, cell viability was determined using an adenosine triphosphate (ATP) monitoring system based on firefly luciferase (CellTiter-Glo® 3D Cell Viability Assay, Promega, Madison, WI) and 3D-live cell staining (Calcein AM, Invitrogen, Carlsbad, CA), according to manufacturer's protocol. Briefly, the assay mixture was prepared in an ATP monitoring system by adding 20 µL of CellTiter-Glo® 3D reagent into 60 µL of medium per well. Cells were lysed with an assay mixture by shaking for 5 min, followed by incubation for 25 min at room temperature. Viable cells were estimated using the SpectraMax iD3 Reader (Molecular Devices LLC, San Jose, CA). In the 3D live-cell staining, the staining solution was prepared by adding 1 µL of Calcein AM into 7 mL of DMEM medium. Cells were incubated with staining solution for 1 hour at 37°C in a 5% CO2-humidified atmosphere. Live cell images were acquired using an automatic fluorescence microscope scanner (ASTA Scanner™, Medical & Bio Decision, South Korea)

# Western blot analysis

Total cell lysates were prepared using a cOmplete™ Lysis-M buffer solution (Roche Life Science, Germany) from the Hep3B and HepG2 hepatocellular carcinoma cell lines. Total protein in lysates was quantified using the Bio-Rad Protein Assay Dye Reagent Concentrate (Bio-Rad, Hercules, CA), 10 µg of total protein were loaded onto 4–20% Mini-PROTEAN TGX™ Precast Protein Gels (Bio-Rad, Hercules, CA) and transferred onto iBlot® PVDF gel Transfer Stack membranes (Thermofisher Scientific, Korea). The membranes were blocked with 5% bovine serum albumin (BSA) in Tris-buffered saline containing 0.05% Tween-20 (TBS-T) at room temperature, and incubated with antibodies against AKT (1:1000, Cell Signaling Technology (CST), #4970), phospho-AKT (p-AKT) (Ser473) (1:1000, CST, #4060), Erk 1/2 (1:1000, CST, #4695), phosphor-Erk (p-Erk) 1/2 (Thr202/Tyr204) (1:1000, CST, #4370), mTOR (1:1000, CST, #2983), phospho-mTOR (p-mTOR) (Ser2448) (1:1000, CST, #5536), E-cadherin (1:1000, CST, #3195), Vimentin (1:1000, Abcam, ab137321), ZO-1 (1:1000, Thermofisher, 339188), Occulidin (1:1000, Thermofisher, 331594), and β-actin (1:5000, CST, #4970) at 4°C overnight. After exposing to horseradish peroxidase (HRP)-conjugated secondary antibodies, proteins were visualized using SuperSignalTM West Pico PLUS (Thermofisher Scientific). Protein bands were visualized using a Chemidoc chemiluminescence imaging system (Bio-rad, Hercules, CA) and quantitative densitometry analysis was performed on the bands of protein detected by immunoblot using Image Lab software (Bio-rad, Hercules, CA) and normalized to β-actin which served as a loading control.

# High Content Image Analysis

Cells were fixed in 2% formaldehyde for 40 min and further incubated with 0.25mg/ml NaBH4 for an additional 40 min. Exposure to primary antibodies against E-cadherin (1:250), Fibronectin (1:250), and ZO-1 (1:200) was done at 4°C for 2 days. After blocking non-specific binding using 5% BSA for 1 h, visualization was done using secondary antibodies conjugated with Alexa Fluor 594 (1:1000, Thermo Scientific, A27016). F-actin was stained with rhodamine phalloidin (1:1000, Invitrogen, R415). Samples

were counterstained with DAPI (1:1000, Thermo Scientific, H3570) and subjected to confocal microscopy (LSM 780, Carl Zeiss, Oberkochen, Germany).

## Cytokine Assay

The expression levels of cytokines and chemokines were analyzed using a Human Cytokine Antibody Array (C5) (RayBiotech, GA). According to the manufacturer's instructions, antibody-embedded membranes were incubated with 1 ml of conditioned media (CM) at 4°C overnight, followed by incubation with HRP-streptavidin at room temperature. Proteins were then visualized using a Chemidoc chemiluminescence imaging system (Bio-rad, Hercules, CA) and chemiluminescent substrate reagent. The signal intensities were quantified using Image lab software (Bio-rad, Hercules, CA).

## Drug Penetration Assay

DOX was used to evaluate drug accumulation in spheroids because of its fluorescent properties. After 1 d of culture, media was replaced with DOX containing media (300 μM). After 12 h of exposure, the 3D cultured cells were washed with PBS before imaging to remove background fluorescence noise. Optical sections were acquired at 10 μm intervals and stacked into a Z-projection from which fluorescence intensity was calculated.

# Results

## Quantitative analysis of the 3D cell-forming uniformity in each 3D cell model

When analyzing the coefficient of variation (CV) value of the DSM model using the 96-pillar plate for 3D cell culture of this study, the CV value was 2.92 % after 1 day of culture, showing high dispensing uniformity and reproducibility as shown in (Fig. 3-a). Similarly, the ASM model had a CV value of 7.89 %, which was confirmed to be of suitable quality for high-throughput screening analysis for drug discovery as shown in (Fig. 3-b).

## High-Throughput screening of six anti-cancer drugs responses in each 3D-cell model

Two types of 3D cell models were implemented and then stabilized for 1 d. After the 1 d stabilization, the drugs were applied, and additional 3D cell culture was performed for 6 d. All drugs indicated higher drug resistance in the ASM model. When HepG2 cells were treated with 5-FU, the $IC_{50}$ values of the DSM model and ASM model were confirmed to be 1.78 μM and more than 100 μM, respectively as shown in (Figs. 4-a and -b). In addition, when Hep3B cells were treated with 5-FU, the $IC_{50}$ values of the DSM model and ASM model were confirmed to be 14.5 μM and 87.6 μM, respectively as shown in (Figs. 4-c and -d).

Lenvatinib, an inhibitor of VEGFR 1–3, FGFR 1–4, PDGFR α, RET, and KIT, showed differences in drug response when comparing the 2D HTS and 3D cell model results. When HepG2 cells were treated with

Lenvatinib, the $IC_{50}$ values of the DSM model and ASM model were confirmed to be 21.77 μM and over 100 μM, respectively as shown in (Figs. 4-a and -b). Lenvatinib dramatically inhibited the Hep3b cell viabilities in 2D HTS conditions under the 1.4 μM $IC_{50}$ value as shown in (Table 1). However, in the 3D cell models, DSM and ASM, Lenvatinib showed no response, and $IC_{50}$ values measured over 100 μM (Figs. 4-c and -d).

# Western blot analysis of epithelial cell markers and cell proliferation receptor protein expression

As shown in (Fig. 6), we performed western blot analysis by recovering cells cultured in 2D and 3D cell models (DSM and ASM). P-Akt was overexpressed in the ASM model, where HepG2 and Hep3B had 3.39-fold and 1.05-fold as compared to the 2D, respectively. These values indicated there was a higher p-Akt expression in the ASM model than in the corresponding 2D and DSM cell culture model conditions. Similarly, the ASM model of HepG2 and Hep3B cells had higher levels of p-Erk expression in the ASM model, HepG2 and Hep3B had levels of 3.14-fold and 2.33-fold as compared to the 2D, respectively (Fig. 6-b). E-cadherin was overexpressed in the ASM model, where HepG2 and Hep3B had values of 6.88-fold and 3.21-fold as compared to the 2D, respectively (Figs. 6-c and -d). These amounts were greater than those found in the 2D and DSM cell culture model conditions. Similarly, the ASM model of HepG2 and Hep3B cells had higher levels of tight junction markers (ZO-1 and Occludin) and ECM marker (Fibronectin) expression in the ASM model where HepG2 and Hep3B had values of 2.58-fold, 6.69-fold, 4.21-fold, 1.48-fold, 3.63-fold and 1.55-fold as compared to the 2D, respectively (Figs. 6-e and -f). β-actin, established as unchanged in each of the three cell culture models, was used as a loading control for immunoblot assay. The quantitatively analyzed densitometry graphs for these immunoblots are displayed in (Fig. 6).

# High Content image analysis of epithelial cancer cell protein and drug penetration related proteins expression

We conducted immunofluorescence analysis for E-cadherin, fibronectin and ZO-1. In the ASM model E-cadherin was overexpressed, where HepG2 and Hep3B had values of 2.66-fold and 1.86-fold as compared to the 2D, respectively (Fig. 7-a). As shown in (Figs. 7-b and -c), the expression level of fibronectin was measured as 1.56-fold and 2.13-fold as compared to the 2D in HepG2 and Hep3B, more than in the corresponding 2D and DSM cell culture models, respectively. Additionally, the expression level of ZO-1 was measured as 1.81-fold and 3.44-fold as compared to the 2D in HepG2 and Hep3B, more than the 2D and DSM cell culture models, respectively.

# Cytokine secretion analysis related to cell proliferation and drug resistance

We recovered the cell culture medium in 2D cell culture and 3D cell models (DSM and ASM) and quantitatively analyzed the secreted cytokines. Among the secreted cytokines, those corresponding to the top 30% in the ASM model were selected. These cytokines had more than a 2-fold increase when

compared to the 2D cell culture condition as shown in (Fig. 8-a). Cell-to-cell interactions in HepG2 in the ASM model stimulated cancer cell interaction, angiogenesis, ECM regulation, immune cell recruitment, and activation via paracrine signaling of Interleukin (IL)-8, IL-15, Transforming growth factor-β (TGF-β), VEGF-A, Chemokine ligand 2 (CCL2), CCL5, CCL17, Chemokine (C-X-C motif) ligand 7 (CXCL7), CXCL8, CXCL10, CXCL13, Insulin-like growth factor-binding protein-1 (IGFBP-1), IGFBP-2, osteopontin (OPN), angiogenin, tissue inhibitors of metalloproteinases-1 (TIMP-1), and TIMP-2, all of which were increased in the ASM model when compared to 2D and DSM model conditions.

Hep3B cells cultured in ASM model stimulate cancer cell interaction, angiogenesis, ECM regulation, immune cell recruitment, and activation via paracrine signaling of IL-8, IL-15, TGF-beta, VEGF-A, CCL2, CCL17, CXCL1, CXCL5, CXCL13, IGFBP-2, OPN, angiogenin, TIMP-1, TIMP-2, stromal cell-derived factor 1 (SDF-1), tumor necrosis factor-a (TNF-a), and TNF-b, all of which were increased in the ASM model when compared to the 2D and DSM model conditions (Fig. 8-b).

# Drug penetration assay for validation of drug resistance in the ASM model using an auto-fluorescent drug

We investigated the penetration behavior of DOX in DSM and ASM models as shown in (Fig. 9). DOX, which is widely used in clinical practice and has its own orange-red fluorescence (excitation 488 nm, emission 517–614 nm), was chosen as a low-molecular-weight antitumor agent. We treated the cells with DOX for 12 h at 300 μM dosage. Representative spheroid cross-sections observed by confocal microscopy are shown in (Fig. 9). The average penetrated areas where the drug fluorescence signals are detectable and at the middle Z-position of 3D cancer spheroids were normalized by the total area of ROI.

The penetrated DOX fluorescence was detected at 14.69 % and 72.2 % in the HepG2 DSM and ASM models respectively (Fig. 9-a). In the Hep3B DSM and ASM models, the penetrated DOX fluorescence was detected at 5.75 % and 86.37 % respectively as shown in (Fig. 9-b).

# Discussion

In this study, we established 3D *in vitro* cancer spheroid models (DSM and ASM) that are advantageous for target discovery and drug screening because they recapitulate important characteristics of in vivo tumors and the tumor microenvironment. Based on our previously developed 3D cell culture platforms by means of a Pillar/well plates, we established a 3D-HCC cancer models that can well maintain the physiological characteristics of HCC cancer cells. A549-eGFP-Puro is a LV-eGFP-PGK-Puro (LV031)-transduced polyclonal population derived from human lung carcinoma cell line A549. To achieve stable reporter expression in the polyclonal population, the cells were selected using puromycin. Since this cell line does not require an additional 3D live cell staining step, we verified the uniformity of cell dispensing in the DSM and ASM models through measurement of the area of A549_GFP cells expressing green fluorescence in the live cell state. To determine a robust and reproducible assay, a means coefficient of

variation (CV) value of less than 10% is used for a good cell-based assay [31]. When analyzing the CV values of two 3D cancer spheroid models, the CV values was under the 10 % respectively. Also, when observing the morphology of the 3D live cells cultured in each 3D cell model, the 3D cultured cells are attached to the surface of the 96-pillar plate in the DSM model. Conversely, in the ASM model, a dramatic morphological difference was observed in which 3D cultured cells formed as a single spheroid morphology in the ASM model. (white arrows mean 3D cultured live cells in each 3D cell models as shown in (Figs. 3-a and -b).

After establishing the reproducibility and uniformity of 3D cancer spheroid models for HTS analysis, we selected drugs that are commonly used for HCC patients in the clinics, particularly drugs targeting VEGFR, tyrosine-protein kinase Met (c-Met), mitogen-activated protein kinases/extracellular signal-regulated kinases (Ras/Raf/MEK/ERK), PDGFR-β, and those that cause DNA/RNA synthesis damage, etc. All drugs were in phase III or IV trials or were approved oncology drugs from public data provided by the US Food and Drug Administration (FDA). The six drugs selected (including three controls) were dispensed into 96-well plates in a dose-dependent manner. Five of the six drugs were treated and diluted three times from 100 μM as the highest concentration in a dose-dependent manner. For DOX, if it was treated at the highest concentration of 100 μM, the drug efficacy would be too high and we would not be able to analyze the $IC_{50}$ value of the doxorubicin. Therefore, the highest concentration was set to 1.56 μM. After the drug treatment, we analyzed the 3D cell viability through the 3D Calcein AM live cell staining method, and by quantitatively measuring the area of the 3D live cells. The efficacy of each drug showed a striking difference between the two 3D cell models, which were quantitatively analyzed by $IC_{50}$ values as shown in (Fig. 4 and Table 1). We found that 5-FU targeting DNA/RNA synthesis inhibition drugs severely inhibited the HepG2 cell viability in 2D HTS and DSM model conditions. Conversely, the ASM model showed no response based on $IC_{50}$ values at 100 μM for the 5-FU drug treatment (Table 1). In addition, when Hep3B cells were treated with 5-FU, the ASM model showed approximately six times higher drug resistance compared to the DSM model. The current study demonstrated that HepG2 and Hep3B cells acquire substantial resistance to 5-FU when the cell-to-cell and cell-to-ECM interactions are re-established in a 3D ASM model (Fig. 5). Thus, in the conventional 2D cell culture model, low doses of 5-FU can induce massive cell death and the drug response results of the 2D cell culture model could be mismatched when compared to actual clinical treatment results. These additional ECM compositions may influence drug response through altered local drug availability, by affecting the expression of drug targets, or by changing intrinsic cellular defense mechanisms such as increased repair upon DNA damage or evasion of apoptosis [32].

We conducted a molecular study to verify differences in drug resistance and the maintenance of the original epithelial characteristics of the two HCC cancer cells according to the 3D cell models when compared to the conventional 2D cell culture method. p-Akt and p-Erk activities, which are known to be related to cell proliferation and important components of cell survival pathways [33], had the greatest increase in the ASM model compared to the 2D and DSM cell culture models (Fig. 6-a). HCC cell lines HepG2 and Hep3B were both classified as epithelial based on their expression of E-cadherin protein and

mRNA [34]. However, the epithelial characteristics of HCC cells were not well maintained in the 2D cell culture and the DSM model. Conversely, in the ASM model, the expression of E-cadherin, an epithelial marker, was relatively high. ZO-1 and Occludin, both of which are tight junction markers, could be identified when the 3-dimensional structure was formed (Figs. 6-e and -f). Interestingly, Fibronectin, a high-molecular-weight glycoprotein of ECM, was overexpressed in the ASM model. It has been reported that Fibronectin was observed in drug-resistant tumor tissues [35]. Fibronectin production occurred in the actual tumor microenvironment and appeared to promote drug resistance [36, 37]. Given these findings, we confirmed that the ASM model implemented in this study has the advantage of maintaining the actual cell characteristics more efficiently than the conventional 2D cell culture method.

The current study demonstrated differences in drug response and protein expression through the HTS and western blot assay in each cell culture model. We also conducted immunofluorescence analysis for E-cadherin, an epithelial cancer cell marker, as well as fibronectin, an ECM marker, and ZO-1 which is a tight junction marker. Since HCC cells have epithelial properties, it can be assumed that culture conditions in which epithelial markers are well expressed can maintain the actual tumor characteristics well. The epithelial characteristics of HCC cells were not well maintained in the 2D cell culture and the DSM model. However, in the ASM model E-cadherin was overexpressed as compared to the 2D. These levels were greater than those in the corresponding 2D and DSM cell culture model counterparts as shown in (Fig. 7-a). Fibronectin plays a crucial role in growth, differentiation, adhesion, and migration [38]. Additionally, production of fibronectin promotes drug resistance and protects from apoptosis induced by chemotherapeutic drugs when compared to those that were grown on plastic [39]. Loss of E-cadherin increases tight junction permeability and alters the localization of ZO-1 [40]. Therefore, the decrease in the expression of the tight junction marker ZO-1 allows for increased drug delivery into cancer cells. The expression levels of the ECM component and structure of tight junctions were measured by immunostaining for fibronectin and ZO-1 to understand the differences of the drug response in each cell culture model as shown in (Figs. 7-b and -c). Fibronectin and ZO-1 were not well expressed in the 2D cell culture and DSM models. However, in the ASM model, these components which are related to the drug resistance were well maintained.

Also, secreted cytokines were analyzed to understand differences in drug resistance and phenotypic characteristics of the two HCC cancer cells according to the 2D and 3D cell models (Fig. 8). HepG2 and Hep3B cells cultured in ASM model stimulate cancer cell-to-cell interaction, angiogenesis, ECM regulation, immune cell recruitment, and activation via paracrine signaling, all of which were increased in the ASM model when compared to the 2D and DSM model conditions. These results indicated that the ASM model implemented in this study has the advantage of maintaining the actual HCC cell characteristics. We analyzed the different penetration behavior of DOX in DSM and ASM models. Therefore, the difference in drug permeability causes a difference in the drug response.

# Conclusions

We tested two *in vitro* 3D cancer spheroid models (DSM and ASM) of HCC cells using 96-pillar/well plates. We cultured cells and created spheroids by either aggregating and diffusing cells in Matrigel attached on the tip of a 96-pillar plate. According to the initial cell position in Matrigel, two 3D-HCC cancer *in vitro* models (DSM and ASM) were established. Among them, the ASM showed high resistance to drugs that were related to the high expression of cancer proliferation, ECM/tight junction markers, and epithelial markers. Additionally, we found that ASM secreted more cytokines related to ECM regulation (TIMP02) and cancer interaction (Il-8, TGF beta 2). The ASM showed lower drug penetration compared to DSM. Overall, the proposed ASM better recapitulates the tumor microenvironment, demonstrating the involvement of the ECM/tight junctions in the cell-to-cell signaling processes. This provides more instructive data for *in vitro* screening of tumor cells.

# Abbreviations

ASM: Aggregated spheroid model

CM: Conditioned media

CV: Coefficient of variation

CCL: Chemokine ligand

CXCL: Chemokine (C-X-C motif) ligand

DSM: Diffused spheroid model

DRC: Dose-response curve

DOX: Doxorubicin

ECM: Extracellular matrix

FGFR: Fibroblast growth factor receptor

HCC: Hepatocellular carcinoma

HTS: High-throughput screening

IL: Interleukin

IGFBP: Insulin-like growth factor-binding protein

OPN: Osteopontin

PDGFR: Platelet-derived growth factor receptor

p-AKT: Phosphorylation-AKT

p-Erk: Phosphorylation -Erk

p-mTOR: Phosphorylation -mTOR

TIMP: Tissue inhibitors of metalloproteinases

TGF-β: Transforming growth factor-β

VEGFR: Vascular endothelial growth factor receptors

2D: Two-dimensional

3D: Three-dimensional

5-Fluorouracil (5-FU)

## Declarations

# Ethics approval and consent to participate

Not applicable

# Consent for publication

Not applicable

# Availability of data and materials

All data generated or analysed during this study are included in this published article and its supplementary information files

# Competing interests

The authors declare that they have no competing interests.

# Funding

This research was supported by A*STAR Industry Alignment Fund Pre-Positioning Fund (HBMS domain): H17/01/a/003, the National Medical Research Council (NMRC) Clinician Scientist Award Senior Investigator (SI) Catergory; NMRC/CSA-SI/0018/2017, the National Research Foundation of Korea(NRF) grant funded by the Korea government(MSIT) (No. 2020R1I1A3066550), the Korea Medical Device

Development Fund grant funded by the Korea government (the Ministry of Science and ICT, the Ministry of Trade, Industry and Energy, the Ministry of Health & Welfare, the Ministry of Food and Drug Safety) (NTIS Number: 202012E15-04)

# Author’s contributions

Conceptualization, S.-Y.L, D.W.L and D.-H.N.; methodology, S.-Y.L, B.K., H.J.H, D.W.L and D.-H.N.; validation, S.-Y.L, D.W.L and D.-H.N; formal analysis, S.-Y.L, D.W.L and D.-H.N; writing—original draft preparation, S.-Y.L, Y.T., M.S., D.W.L and D.-H.N; writing—review and editing, S.-Y.L, Y.T., M.S., V.T., P.K.-H.C., D.W.L and D.-H.N.; supervision, D.W.L and D.-H.N.; project administration, D.W.L and D.-H.N.; All authors have read and agreed to the published version of the manuscript.

# Acknowledgments

Not applicable

## References

1. El-Serag HB. Hepatocellular carcinoma. N Engl J Med. 2011;365:1118-27.
2. Lachenmayer A, Alsinet C, Chang CY, Llovet JM. Molecular approaches to treatment of hepatocellular carcinoma. Dig Liver Dis. 2010;42:264-72.
3. Feitelson MA, Sun B, Tufan NLS, Liu J, Pan J, Lian Z. Genetic mechanisms of hepatocarcinogenesis. Oncogene 2002;21:2593-604.
4. Llovet JM, Ricci S, Mazzaferro V, Hilgard P, Gane E, Blanc J-F, et al. Sorafenib in advanced hepatocellular carcinoma. N Engl J Med. 2008;359:378-90.
5. Cheng A-L, Kang Y-K, Chen Z, Tsao C-J, Qin S, Kim JS, et al. Efficacy and safety of sorafenib in patients in the Asia-Pacific region with advanced hepatocellular carcinoma: a phase III randomised, double-blind, placebo-controlled trial. lancet Oncol. 2009;10:25-34.
6. Bruix J, Qin S, Merle P, Granito A, Huang Y-H, Bodoky G, et al. Regorafenib for patients with hepatocellular carcinoma who progressed on sorafenib treatment (RESORCE): a randomised, double-blind, placebo-controlled, phase 3 trial. Lancet. 2017;389:56-66.
7. Tang W, Chen Z, Zhang W, Cheng Y, Zhang B, Wu F, et al. The mechanisms of sorafenib resistance in hepatocellular carcinoma: theoretical basis and therapeutic aspects. Signal Transduct Target Ther. 2020;5:1-15.
8. Gholam P. The role of sorafenib in hepatocellular carcinoma. Gastroenterol Hepatol. 2015;11:253-5.
9. Mross K, Frost A, Steinbild S, Hedbom S, Büchert M, Fasol U, et al. A phase I dose–escalation study of regorafenib (BAY 73–4506), an inhibitor of oncogenic, angiogenic, and stromal kinases, in patients with advanced solid tumors. Clin Cancer Res. 2012;18:2658-67.

10. Strumberg D, Scheulen M, Schultheis B, Richly H, Frost A, Büchert M, et al. Regorafenib (BAY 73-4506) in advanced colorectal cancer: a phase I study. Br J Canc. 2012;106:1722-27.
11. Tsai J-J, Pan P-J, Hsu F-T. Regorafenib induces extrinsic and intrinsic apoptosis through inhibition of ERK/NF-κB activation in hepatocellular carcinoma cells. Oncol Rep. 2017;37:1036-44.
12. Edmondson R, Broglie JJ, Adcock AF, Yang L. Three-dimensional cell culture systems and their applications in drug discovery and cell-based biosensors. Assay Drug Dev Technol. 2014;12:207-18.
13. Birgersdotter A, Sandberg R, Ernberg I. Gene expression perturbation in vitro—a growing case for three-dimensional (3D) culture systems. Semin Cancer Biol. 2005;15:405-12.
14. Weaver VM, Petersen OW, Wang F, Larabell C, Briand P, Damsky C, et al. Reversion of the malignant phenotype of human breast cells in three-dimensional culture and in vivo by integrin blocking antibodies. J Cell Biol. 1997;137:231-45.
15. Bhadriraju K, Chen CS. Engineering cellular microenvironments to improve cell-based drug testing. Drug Discov Today. 2002;7:612-20.
16. Song Y, Kim J-S, Kim S-H, Park YK, Yu E, Kim K-H, et al. Patient-derived multicellular tumor spheroids towards optimized treatment for patients with hepatocellular carcinoma. J Exp Clin Cancer Res. 2018;37:109.
17. Shield K, Ackland ML, Ahmed N, Rice GE. Multicellular spheroids in ovarian cancer metastases: Biology and pathology. Gynecol Oncol. 2009;113:143-48.
18. Zietarska M, Maugard CM, Filali-Mouhim A, Alam-Fahmy M, Tonin PN, Provencher DM, et al. Molecular description of a 3D in vitro model for the study of epithelial ovarian cancer (EOC). Mol Carcinog. 2007;46:872-85.
19. Le Roux L, Volgin A, Maxwell D, Ishihara K, Gelovani J, Schellingerhout D. Optimizing imaging of three-dimensional multicellular tumor spheroids with fluorescent reporter proteins using confocal microscopy. Mol Imaging. 2008;7:214-21.
20. Tung Y-C, Hsiao AY, Allen SG, Torisawa Y-S, Ho M, Takayama S. High-throughput 3D spheroid culture and drug testing using a 384 hanging drop array. Analyst. 2011;136:473-8.
21. Kang J, Lee DW, Hwang HJ, Yeon S-E, Lee M-Y, Kuh H-J. Mini-pillar array for hydrogel-supported 3D culture and high-content histologic analysis of human tumor spheroids. Lab Chip. 2016;16:2265-76.
22. Lee DW, Choi Y-S, Seo YJ, Lee M-Y, Jeon SY, Ku B, et al. High-throughput screening (HTS) of anticancer drug efficacy on a micropillar/microwell chip platform. Anal Chem. 2014;86:535-42.
23. Lee DW, Doh I, Nam D-H. Unified 2D and 3D cell-based high-throughput screening platform using a micropillar/microwell chip. Sensors and Actuators B. 2016;228:523-8.
24. Lee DW, Choi YS, Seo YJ, Lee MY, Jeon SY, Ku B, et al. High-Throughput, Miniaturized Clonogenic Analysis of a Limiting Dilution Assay on a Micropillar/Microwell Chip with Brain Tumor Cells. Small. 2014;10:5098-105.
25. Helgerud T, Gåserød O, Fjæreide T, Andersen P, Larsen C. Food Stabilisers, Thickeners and Gelling. Agents. 2009;4:50-77.

26. Andersen T, Strand B, Formo K, Alsberg E, Christensen B. Alginates as biomaterials in tissue engineering. Carbohydrate Chemistry. 2011;37:227-58.
27. Kenny PA, Lee GY, Myers CA, Neve RM, Semeiks JR, Spellman PT, et al. The morphologies of breast cancer cell lines in three-dimensional assays correlate with their profiles of gene expression. Molecular Oncology. 2007;1:84-96.
28. Kleinman HK, Martin GR. Matrigel: basement membrane matrix with biological activity. Seminars In cancer Biology. 2005;15:378-86.
29. Shaw LM. Tumor cell invasion assays. Cell Migration. 2005;294:97-105.
30. Albini A, Iwamoto Y, Kleinman H, Martin G, Aaronson S, Kozlowski J, et al. A rapid in vitro assay for quantitating the invasive potential of tumor cells. Cancer Res. 1987;47:3239-45.
31. Nebane NM, Coric T, Whig K, McKellip S, Woods L, Sosa M, et al. High-throughput RNA interference screening: Tricks of the trade. J Lab Autom. 2013;18:334-9.
32. Sebens S, Schafer H. The tumor stroma as mediator of drug resistance-a potential target to improve cancer therapy. Curr Pharm Biotechnol. 2012;13:2259-72.
33. Breslin S, O'Driscoll L. The relevance of using 3D cell cultures, in addition to 2D monolayer cultures, when evaluating breast cancer drug sensitivity and resistance. Oncotarget. 2016;7:45745-56.
34. Fuchs BC, Fujii T, Dorfman JD, Goodwin JM, Zhu AX, Lanuti M, et al. Epithelial-to-mesenchymal transition and integrin-linked kinase mediate sensitivity to epidermal growth factor receptor inhibition in human hepatoma cells. Cancer Res. 2008;68:2391-9.
35. Ye Y, Zhang R, Feng H. Fibronectin promotes tumor cells growth and drugs resistance through a CDC42-YAP dependent signaling pathway in colorectal cancer. Cell Biol Int. 2020;9:1840-9.
36. Afasizheva A, Devine A, Tillman H, Fung KL, Vieira WD, Blehm BH, et al. Mitogen-activated protein kinase signaling causes malignant melanoma cells to differentially alter extracellular matrix biosynthesis to promote cell survival. BMC cancer. 2016;16:1-15.
37. Fedorenko IV, Abel EV, Koomen JM, Fang B, Wood ER, Chen YA, et al. Fibronectin induction abrogates the BRAF inhibitor response of BRAF V600E/PTEN-null melanoma cells. Oncogene. 2016;35:1225-35.
38. Pankov R, Yamada KM. Fibronectin at a glance. J Cell Sci. 2002;115:3861-3.
39. Rintoul RC, Sethi T. Extracellular matrix regulation of drug resistance in small-cell lung cancer. Clin Sci. 2002;102:417-24.
40. Tunggal JA, Helfrich I, Schmitz A, Schwarz H, Günzel D, Fromm M, et al. E-cadherin is essential for in vivo epidermal barrier function by regulating tight junctions. EMBO J. 2005; 24:1146-56.

# Table

Due to technical limitations, table 1 is only available as a download in the Supplemental Files section.

# Figures

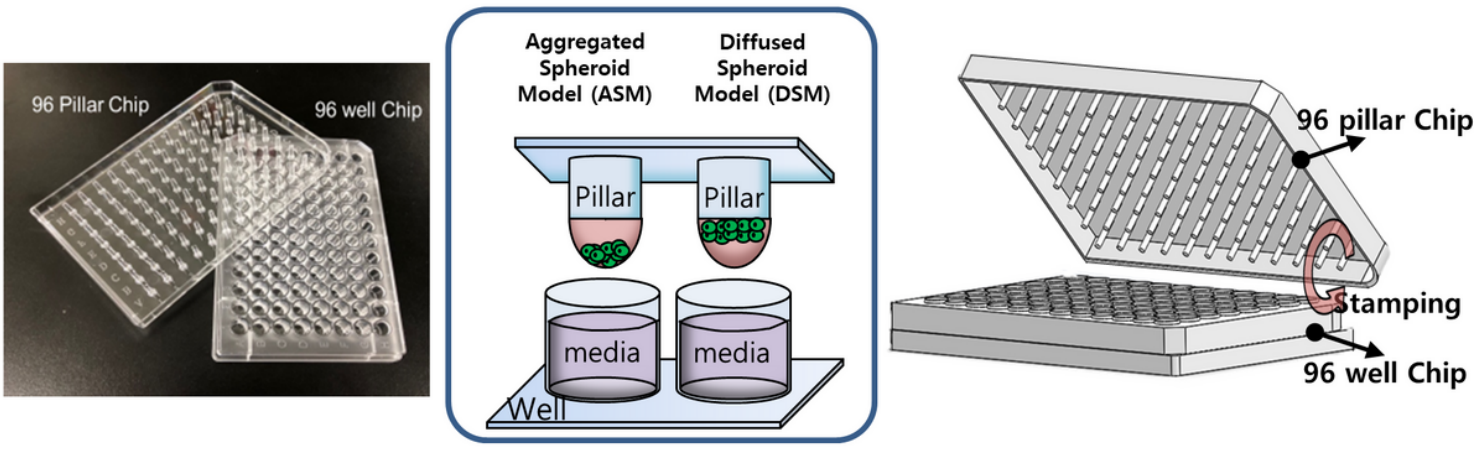


## Figure 1

Schematic view of the 96-pillar/well plate and wet chamber for 3D-HCC cell-based high-throughput screening (HTS). The 3D-HCC cells were cultured three-dimensionally with six different drugs in a 96-pillar/well plate. (seven doses and three replicates)

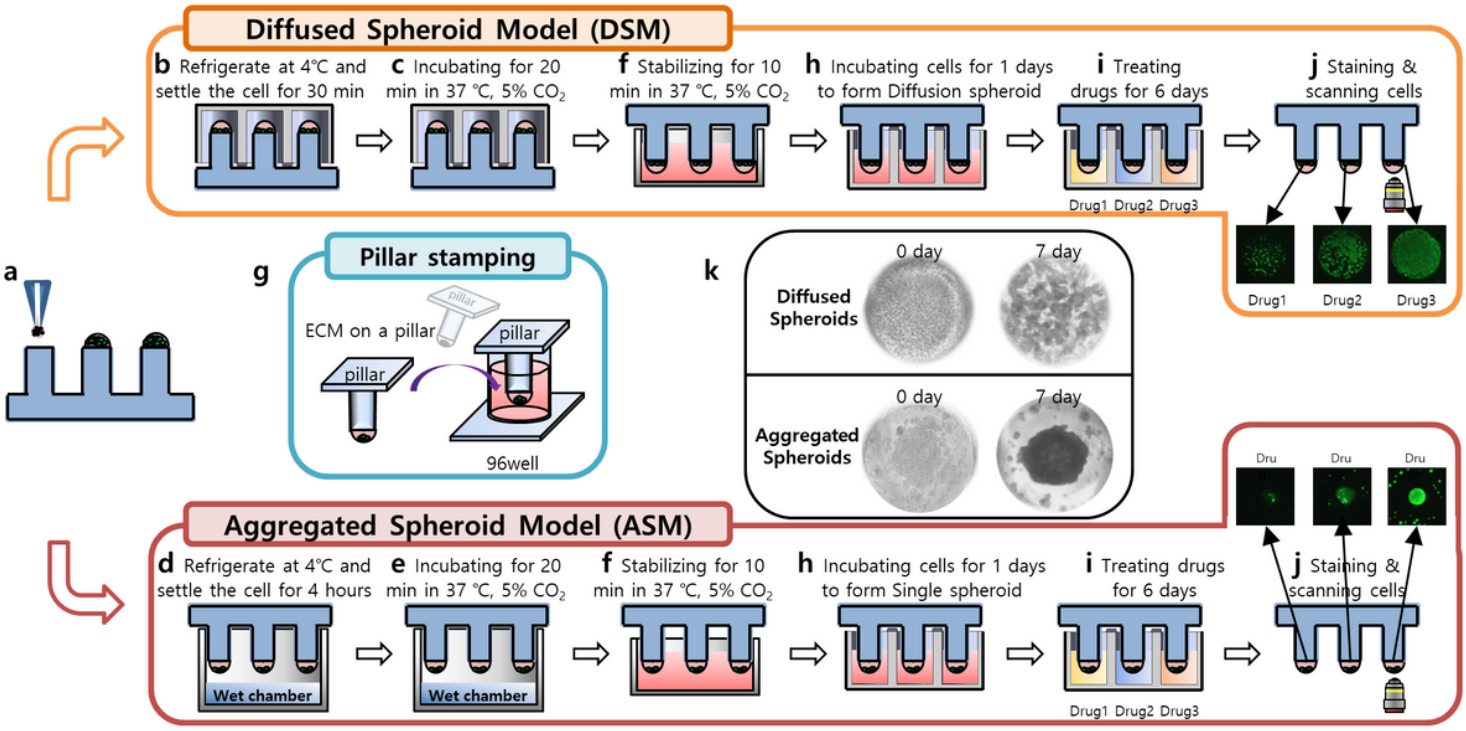


## Figure 2

Experimental procedures of 3D Cell culture model implementation (DSM and ASM) using a 96-pillar/well plate. (a) Cell and Matrigel mixture dispensed on the surface of the 96-pillar plate. (b) 3D cell and Matrigel mixture icing step with the pillar surface facing upward. (c) 3D cell and Matrigel gelation step with the pillar surface facing upward. (d) 3D cell and Matrigel mixture icing step with the pillar surface facing

downward. (e) 3D cell and Matrigel gelation step with the pillar surface facing downward. (f) Additional stabilization step for 10 min. (g) 96-pillar plate stamped with the 96-well plate for 3D cell culture. (h) 1 day incubation for stabilizing the cells by stamping the 96-pillar plate into the 96-well plate filled with cell culture medium. (i) Drug exposure by replacing the 96-well plate with another filled with six different drugs. (j) Green fluorescence image scanning after 3d live cell staining. (k) Representative images for spread 3D cells in the DSM and aggregated 3D cells in the ASM.

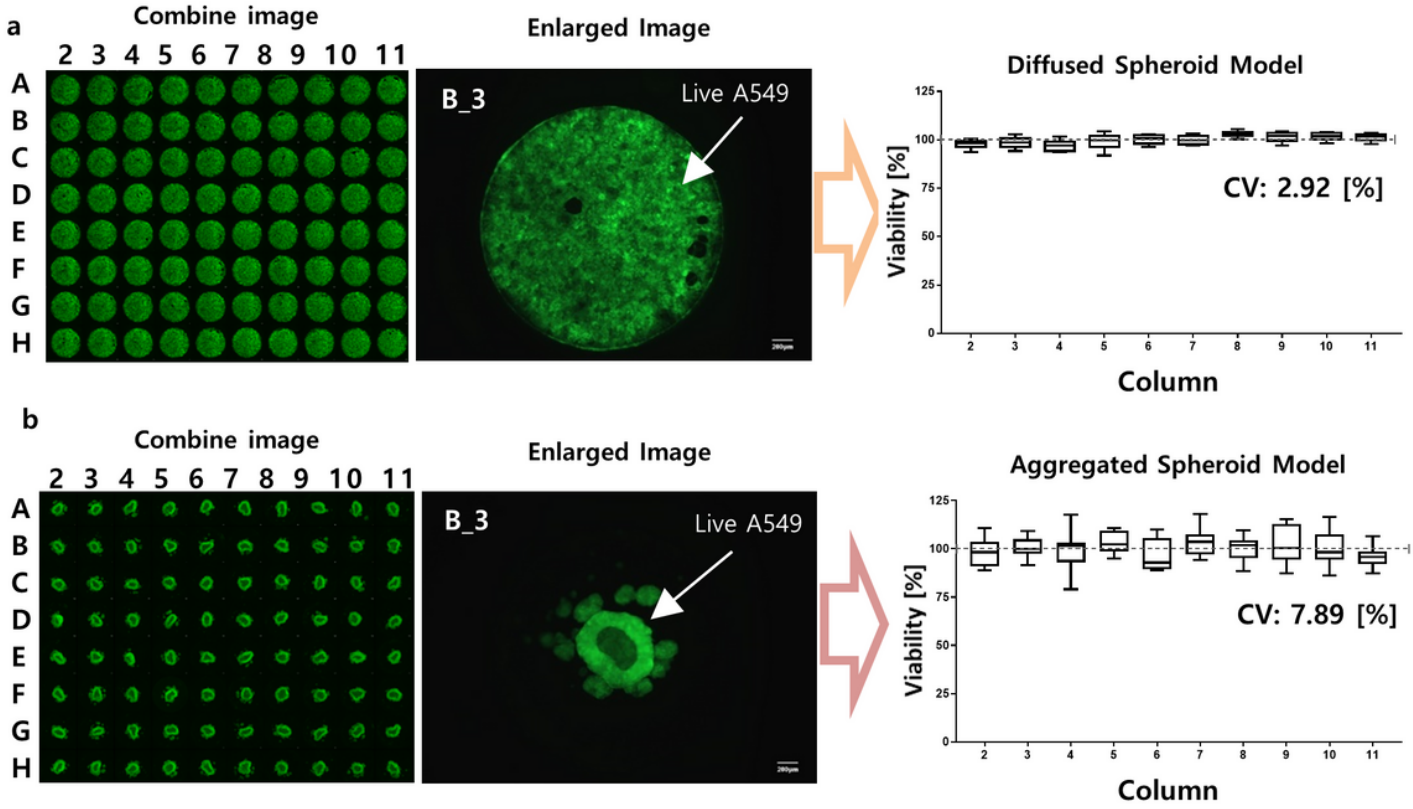


## Figure 3

Quantitative analysis of the 3D Cell forming uniformity. (a) Images of the 3D cell and Matrigel seeding uniformity of DSM (CV: 2.92 %). (b) Images of the 3D cell and Matrigel seeding uniformity of ASM (CV: 7.89 %). White arrow and green fluorescence indicate the live 3d A549 cell.

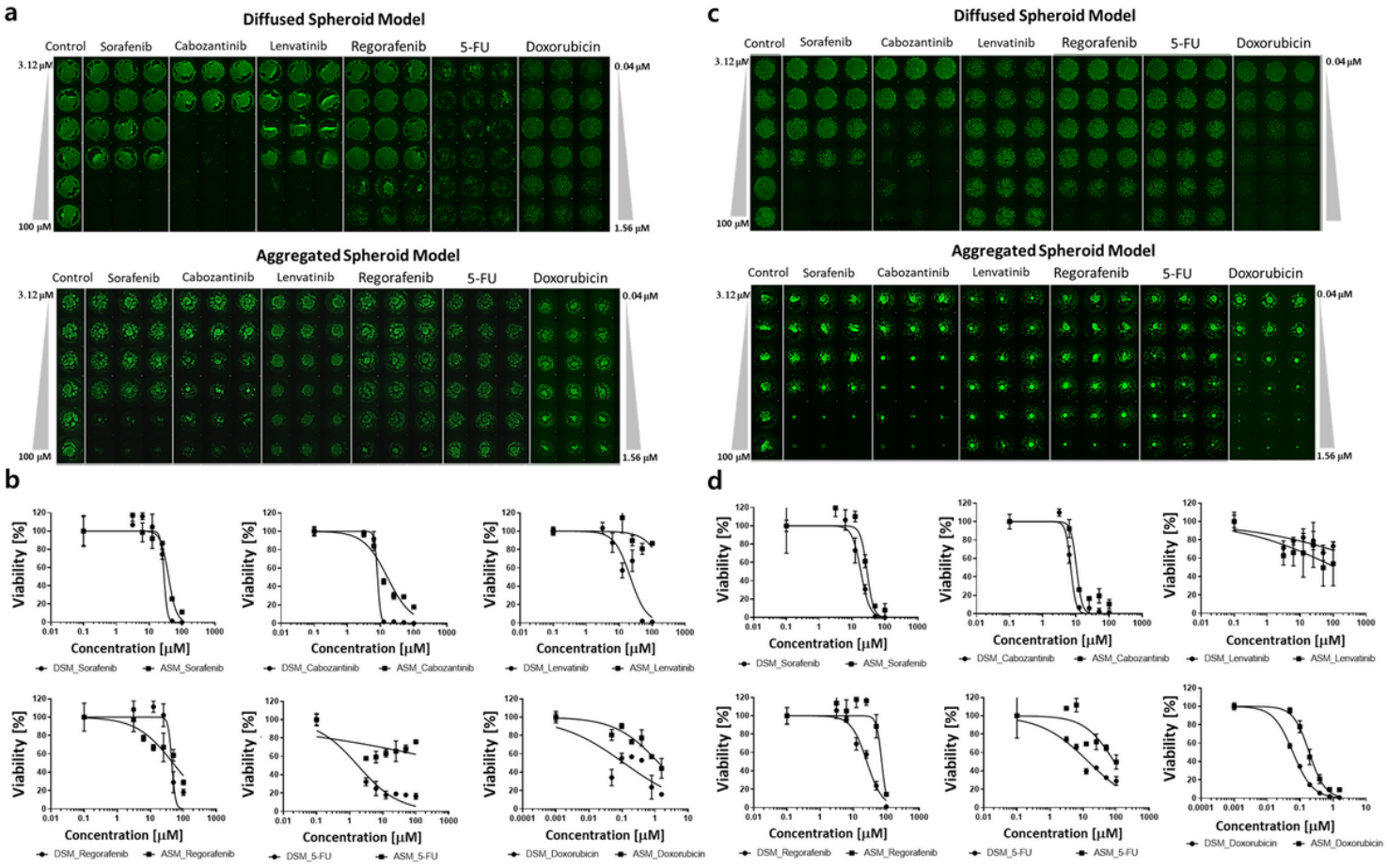


| IC50 | Diffusion Spheroid Model | Aggregated Spheroid Model |
|---|---|---|
| Sorafenib | 28.45 | 39.89 |
| Cabozantinib | 8.11 | 16.08 |
| Lenvatinib | 21.77 | > 100 |
| Regorafenib | 44.79 | 48.58 |
| 5-FU | 1.78 | > 100 |
| Doxorubicin | 0.1152 | 1.305 |

| IC50 | Diffusion Spheroid Model | Aggregated Spheroid Model |
|---|---|---|
| Sorafenib | 18.56 | 28.65 |
| Cabozantinib | 6.99 | 10.35 |
| Lenvatinib | >100 | >100 |
| Regorafenib | 25.88 | 72.86 |
| 5-FU | 14.5 | 87.6 |
| Doxorubicin | 0.061 | 0.188 |

## Figure 4

Comparative dose response curve analysis of six different drugs in 3D cell models. The IC50 was calculated to compare the 3d live cell staining dye expression level according to the dose of each of six drugs. (a) Combined image of 3D live HepG2 cell in the DSM and ASM. (b) Dose response curves and summary table of quantitatively analyzed drug efficacy according to the doses of the six drugs tested in the HepG2 DSM and ASM. (c) Combined image of 3D live Hep3B cells in the DSM and ASM. (d) Dose response curves and summary table of quantitatively analyzed drug efficacy according to the doses of the six drugs tested in the Hep3B DSM and ASM

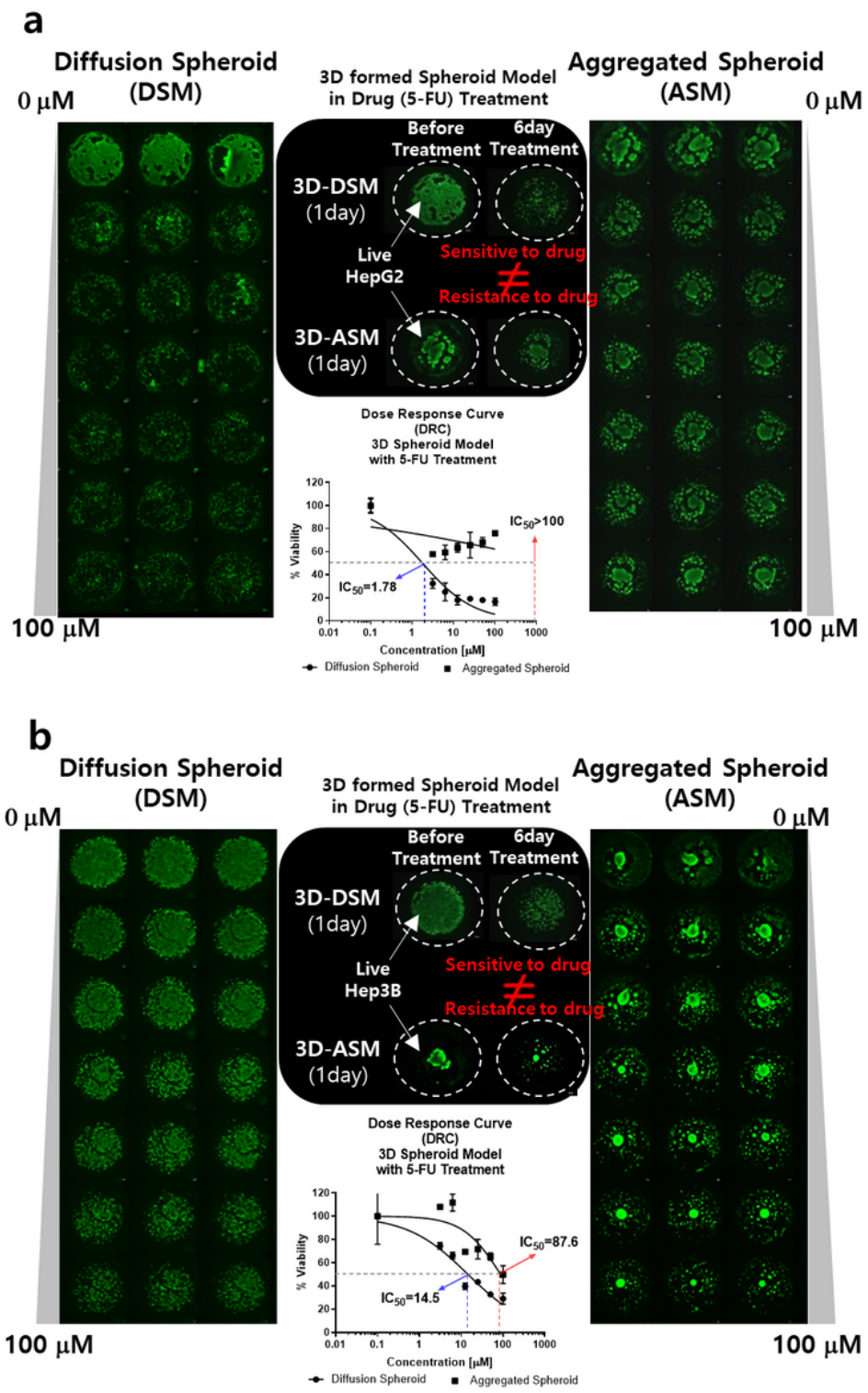


## Figure 5

Comparison of drug responses according to 3D-Live cell images and dose response analysis in 3D cell culture models (DSM and ASM). (a) Representative case of drug response differences in HepG2 DSM and ASM. The IC50 values of the DSM and ASM were calculated at 1.78 μM and more than 100 μM, respectively. (b) Representative case of drug response difference in Hep3B DSM and ASM. The IC50 values of the DSM model and ASM model were calculated at 14.5 μM and 87.6 μM, respectively.

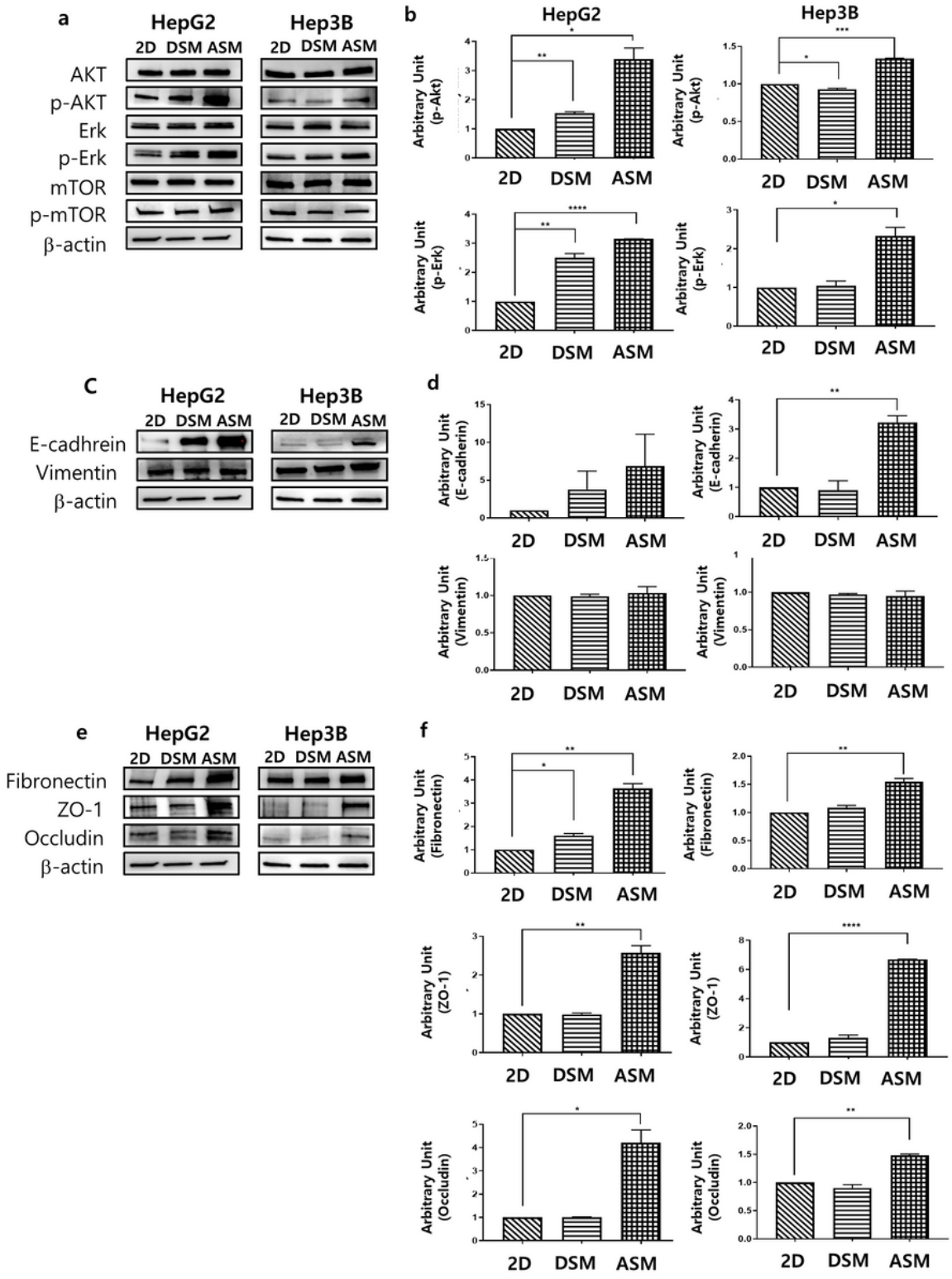


## Figure 6

Western blot analysis of epithelial cell protein and cell proliferation receptor protein expression. Changes in the expression level of proliferation receptor protein (a and b), epithelial cell protein (c and d), ECM, and cell junction protein (e and f) as determined by western blot analysis. Increased expression of p-AKT, p-Erk, E-cadherin, Fibronectin, ZO-1 and Occludin under ASM culture conditions. All factors were normalized to β-actin. *p < 0.05, ** p < 0.01, *** p < 0.001, **** p < 0.0001

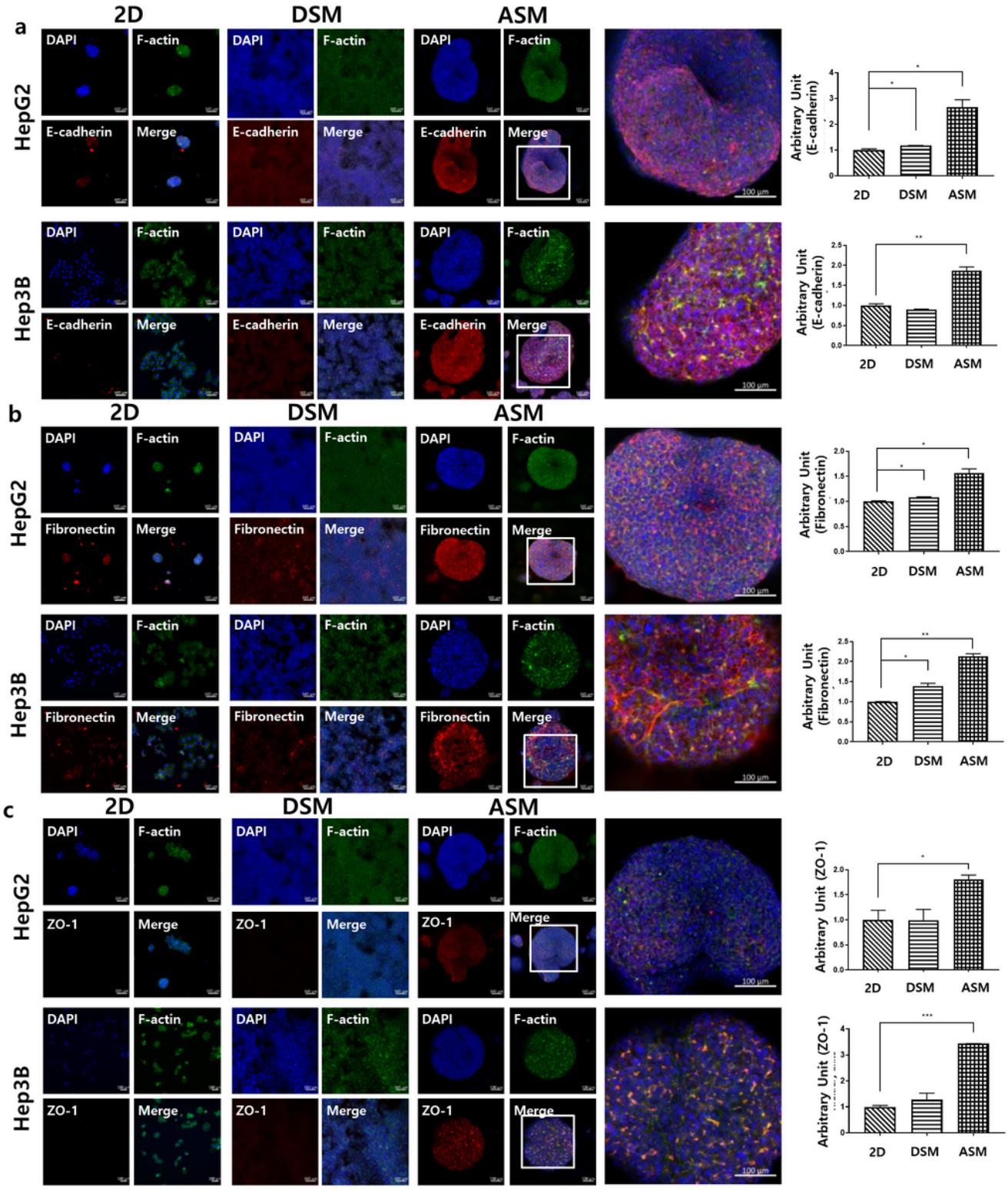


## Figure 7

High-content image analysis of epithelial cancer cell protein and drug penetration related protein expression. The expression of E-cadherin (a), Fibronectin (b) and ZO-1 (c) increased under ASM culture conditions. Optical sections were acquired at 10 μm intervals and stacked into a Z-projection. Scale bars: 100 μm *p < 0.05, ** p < 0.01, *** p < 0.001

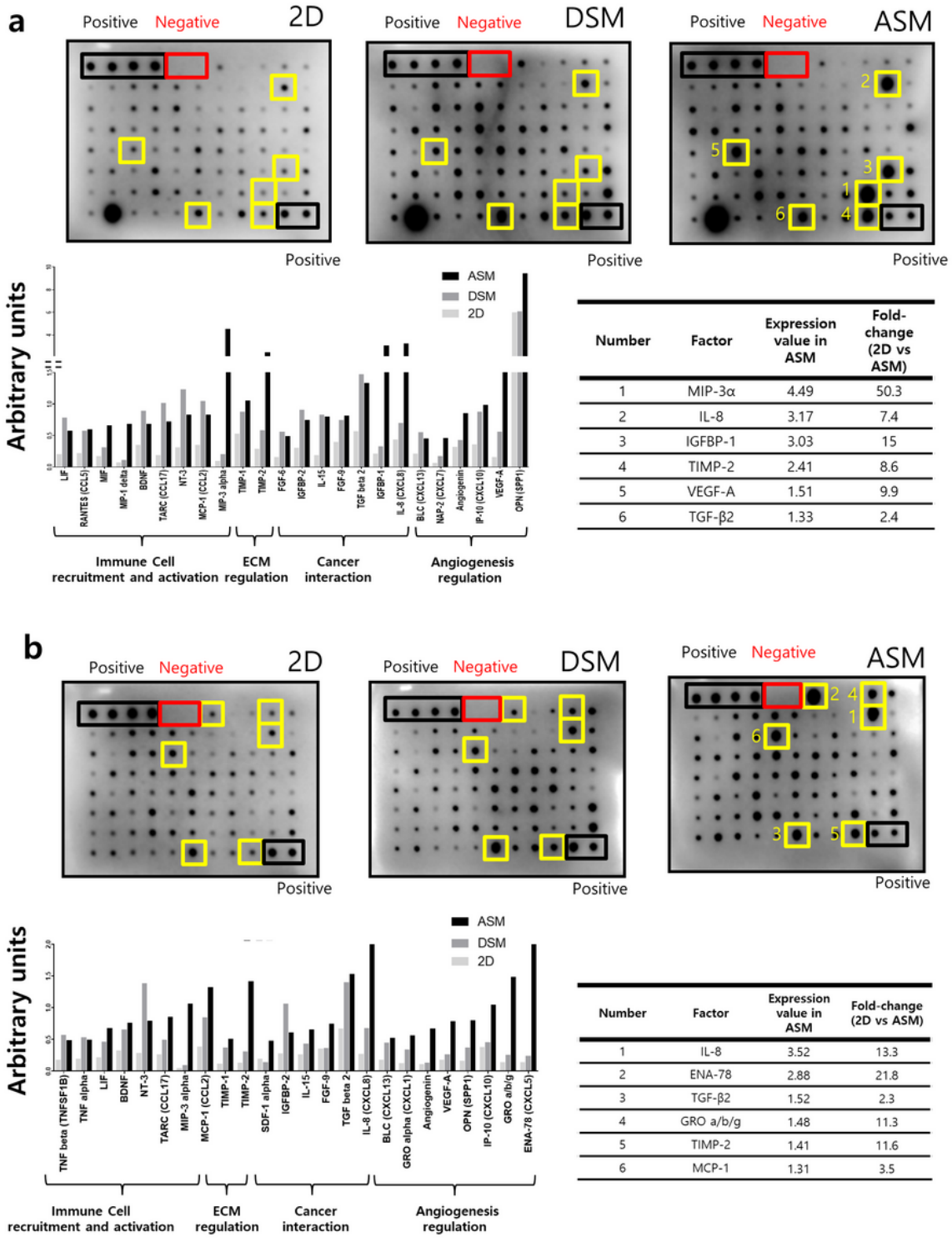


| Number | Factor | Expression value in ASM | Fold-change (2D vs ASM) |
|---|---|---|---|
| 1 | MIP-3α | 4.49 | 50.3 |
| 2 | IL-8 | 3.17 | 7.4 |
| 3 | IGFBP-1 | 3.03 | 15 |
| 4 | TIMP-2 | 2.41 | 8.6 |
| 5 | VEGF-A | 1.51 | 9.9 |
| 6 | TGF-β2 | 1.33 | 2.4 |

| Number | Factor | Expression value in ASM | Fold-change (2D vs ASM) |
|---|---|---|---|
| 1 | IL-8 | 3.52 | 13.3 |
| 2 | ENA-78 | 2.88 | 21.8 |
| 3 | TGF-β2 | 1.52 | 2.3 |
| 4 | GRO a/b/g | 1.48 | 11.3 |
| 5 | TIMP-2 | 1.41 | 11.6 |
| 6 | MCP-1 | 1.31 | 3.5 |

## Figure 8

Cell proliferation and drug resistance related cytokine secretion analysis. Increased secretion of chemokines and cytokines in CM of ASM culture condition. Representative images of human cytokine array analysis in CM of HepG2 (a) and Hep3B (b). Graph indicates factors showing increases to the top 30% in the ASM. Six factors were detected to be the highest under ASM culture conditions (yellow boxes).

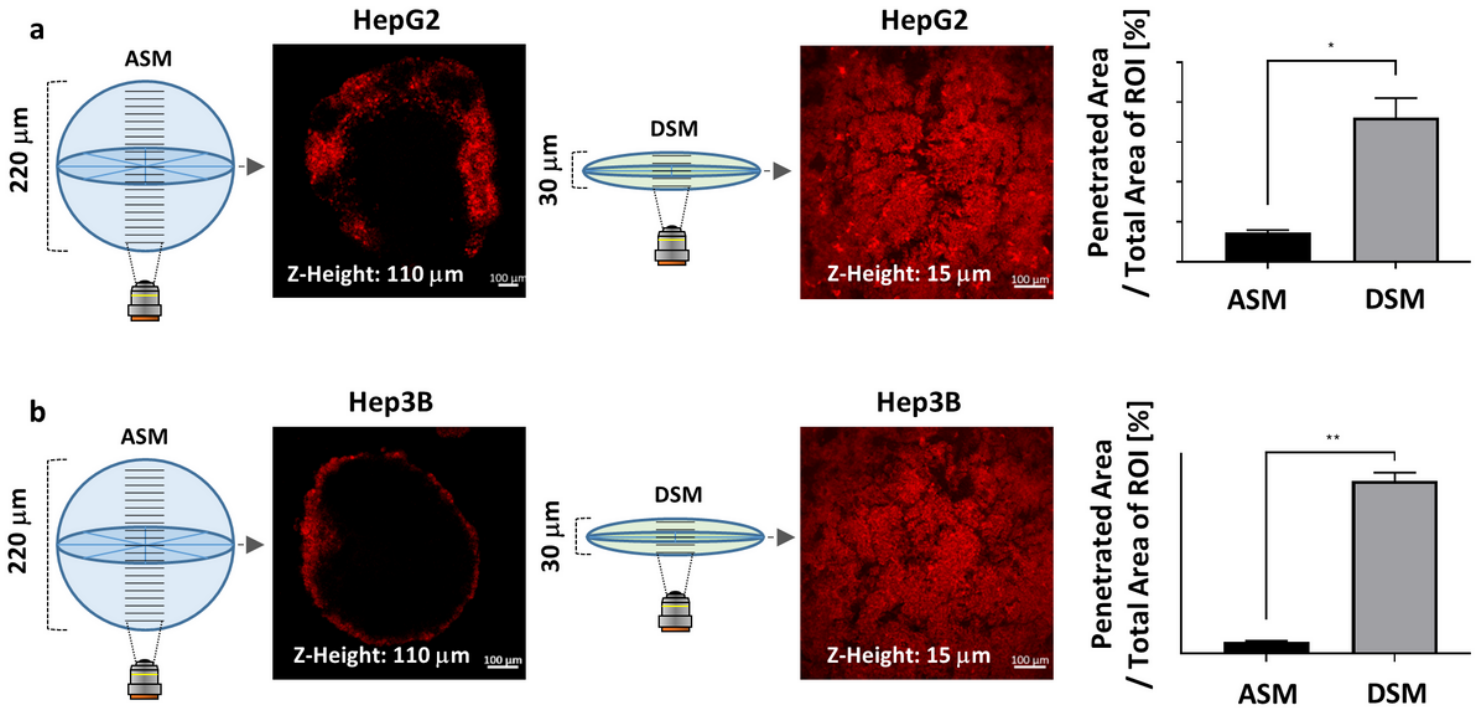


**Figure 9**

Drug penetration assay for validation of drug resistance in the ASM using auto-fluorescent drug (DOX). (a) Images of DOX penetration in HepG2 DSM and ASM and quantitatively analyzed drug penetration ratios in each 3D model. The penetrated DOX fluorescence was calculated at 14.69 % and 72.2 %, respectively. (b) Images of DOX penetration in HepG2 DSM and ASM and quantitatively analyzed drug penetration ratios in each 3D model. The penetrated DOX fluorescence was calculated at 5.75 % and 86.37 %, respectively. Scale bars: 100 µm *p < 0.05, ** p < 0.01

# Supplementary Files

This is a list of supplementary files associated with this preprint. Click to download.

- TableJECCRLeeetal.xlsx